Electron excitation cross sections for the $2s^2 2p\ ^2P^o \rightarrow 2s2p^2\ ^4P$ and $2s2p^2\ ^2D$ transitions in O^{3+}

S. J. Smith,[1] J. A. Lozano,[1] S. S. Tayal,[2] and A. Chutjian[1]
[1]*Jet Propulsion Laboratory, California Institute of Technology, Pasadena, California 91109, USA*
[2]*Department of Physics, Clark Atlanta University, Atlanta, Georgia 30314, USA*
(Received 2 September 2003; published 24 December 2003)

Experimental and theoretical electron-excitation cross sections are reported for the $2s^2 2p\ ^2P^o \rightarrow 2s2p^2\ ^4P$ and $\rightarrow 2s2p^2\ ^2D$ transitions in O^{3+}. The transition energies are centered at 8.85 and 15.7 eV, respectively. Measurements are made using the energy-loss merged-beams method. The center-of-mass energy range covered is 6.1 (below threshold) to 19.3 eV. Comparison is made with results of new calculations in a 25-state *R*-matrix theory and with results in a previous eight-state *R*-matrix calculation. The presence of rich resonance structure is confirmed in both experiment and theory. In most cases there is good agreement in the magnitude of cross section, and energy location of the resonances.

DOI: 10.1103/PhysRevA.68.062708 PACS number(s): 34.80.Kw

I. INTRODUCTION

Optical emissions from highly charged ions provide important diagnostics of both electron temperature and density in high-electron temperature plasmas. Such plasmas are encountered in solar and stellar atmospheres, shock-heated portions of circumstellar clouds and the interstellar medium, and in planetary magnetospheres (such as the Io torus). Highly charged ions (HCI's) including carbon, nitrogen, oxygen, nickel and iron ions are also present in fusion plasmas as impurities sputtered into the plasma from plasma-wall collisions. In all cases, knowledge of excitation cross sections are required to understand the plasma density and temperature, and to model the cooling rate of the plasma from radiation.

Line intensity ratios for the O^{3+} intercombination multiplets near 1400 Å have been used as electron density-sensitive diagnostics for analysis of solar and stellar transition regions [1–3], novae [4], and quasars [5]. The O^{3+} ground-state fine structure splitting at 25.91 μm has also been used as part of an infrared line intensity ratio (combined with an emission at a nearby wavelength from another species, such as Ne^+) to search for active-galactic nuclei [6]. All upper levels, whether excited in a star or in cooler interstellar regions, are populated predominantly by electron impact. A summary of the O^{3+} energy levels relevant to this work is given in Fig. 1.

Theoretical studies in the O^{3+} system have included calculation of energy levels and collision strengths using the close coupling *R*-matrix theory [7–9], the calculation of energy levels and optical oscillator strengths using a multiconfiguration Hartree-Fock theory [10], and a close-coupling *R*-matrix approach [11].

II. EXPERIMENTAL DETAILS

Measurements of absolute cross sections were carried out at the JPL Highly Charged Ion Facility using a 14.0 GHz electron-cyclotron resonance ion source (ECRIS) and merged-beams system. The experimental details have been previously given in Greenwood *et al.* [12] and Chutjian *et al.* [13]. The arrangement of the facility's beam lines may be found in Smith *et al.* [14]. Briefly, a beam of O^{3+} ions is derived from the ECRIS at an extraction voltage of 7.0 kV, or at a beam energy of $7.0q$ keV$=21.0$ keV. Molecular oxygen was used as the feed gas, with no other supporting gas used. The O^{3+} ions are mass-charge analyzed in a double-focusing 90° bending magnet. The beam is focused into the center of the interaction region through a series of baffled differential-pumping regions and lens systems. The O^{3+} beam is merged with a magnetically confined electron beam, whereby the electrons are trochoidally deflected onto the ion beam. The electrons and ions interact along the 20.0 ± 0.3 cm merged path length. After the interaction, the confined inelastically scattered electrons are then demerged from the ions using a second trochoidal analyzer. Detection is by means of a position sensitive detector at the exit of the second trochoidal system. Beam-overlap profiles are measured with both beams running, and at four locations along the merged path using vanes with circular holes that intersect the

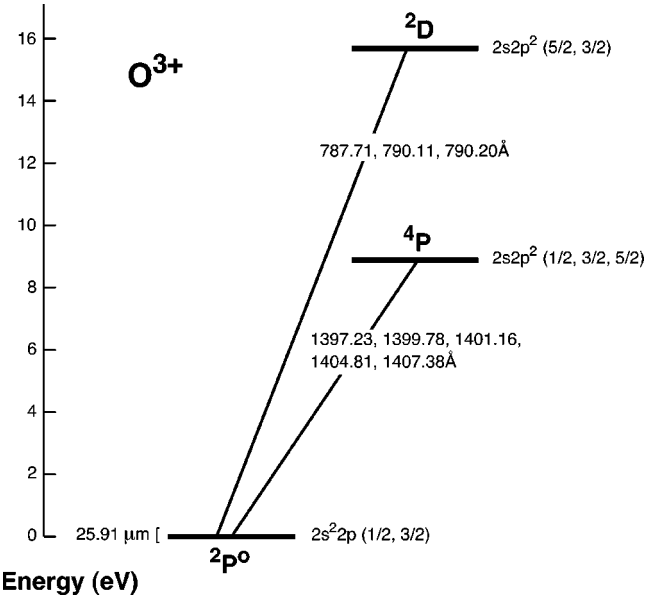

FIG. 1. Energy-level diagram of O^{3+} indicating the fine-structure wavelengths, including the ground-state transition at 25.91 μm useful in galactic infrared line searches. The excitations $2s^2 2p\ ^2P^o \rightarrow 2s2p^2\ ^4P$ and $2s^2 2p\ ^2P^o \rightarrow 2s2p^2\ ^2D$ are studied herein.

beams at different radial distances from the merged axis. Discrimination against elastically scattered electrons is through an electronic aperture that selectively filters electrons with large Larmor radii (i.e., the elastically scattered ones) prior to the trochoidal analyzer [12], and through the use of retarding grids after the analyzer. Any remaining elastically scattered electrons which can overlap the inelastic spectrum are accounted for (and subtracted) through the use of trajectory modeling and elastic differential cross sections $d\sigma_{\rm el}/d\Omega$ calculated from the standard Coulomb-scattering expression for a triply ionized target given as $d\sigma_{\rm el}/d\Omega = 1.166\times10^{-14}\,E^2\sin^4(\theta/2)$ cm^2/sr for center-of-mass angle θ and energy E. These three features, combined with the velocity dispersion of the trochoidal analyzer, allow one to carry out measurements at energies both at and significantly above threshold.

The basic relation between the experimentally measured quantities and the cross section $\sigma(E)$ (cm^2) at energy E is given as

$$\sigma(E) = \frac{\mathsf{R}qe^2\mathsf{F}}{\varepsilon I_e I_i L}\left|\frac{v_e v_i}{v_e - v_i}\right|, \tag{1}$$

where R is the total signal rate (s^{-1}), q is the ionic charge state (here, $q=3$), e is the electron charge (C), I_e and I_i are the electron and ion currents (A) respectively, v_e and v_i are the electron and ion velocities (cm s^{-1}) respectively, L is the merged path length (cm), ε is the combined efficiency of the rejection grids–microchannel-plate detection system (dimensionless), and F is the overlap factor between the electron and ion beams (cm^2). All quantities in Eq. (1) are measured, or for the particle velocities, are determined through their acceleration potentials.

III. THEORETICAL CONSIDERATIONS

The present 25-state R-matrix calculations for electron impact excitation of O^{3+} are performed for the $2s^2 2p\ ^2P^o \rightarrow 2s2p^2\ ^4P$ and ^2D transitions in the low-energy region from threshold to 25 eV to compare with the measured cross sections. Earlier calculations for electron impact excitation of fine-structure transitions were presented by Luo and Pradhan [7] and Blum and Pradhan [8]. They included eight LS states ($2s^2 2p\ ^2P^o$, $2s2p^2\ ^4P$, ^2D, ^2S, ^2P, $2p^3\ ^4S^o$, $^2D^o$, $^2P^o$) in the close-coupling expansion in their R-matrix calculations in LS-coupling and used an algebraic transformation from the LS to a pair-coupling scheme to obtain collision strengths and rates for the fine-structure transitions.

The present calculations take into account electron correlation and coupling to low-lying as well as to higher excited states to obtain accurate theoretical cross sections. Fairly extensive configuration-interaction (CI) wave functions are used to represent the target states. Nine orthogonal one-electron orbitals $1s$, $2s$, $2p$, $3s$, $3p$, $3d$, $4s$, $4p$, and $4d$ describe the target wave functions that have been calculated using the multiconfiguration Hartree-Fock (MCHF) atomic-structure package [15]. The $1s$, $2s$, and $2p$ orbitals were first generated in a simple Hartree-Fock (HF) calculation of the ground $1s^2 2s^2 2p\ ^2P^o$ state. The $2p$ orbital was then reoptimized on the average of the $2p^3\ ^4S^o$, $^2D^o$, and $^2P^o$ states. The spectroscopic $3s$, $3p$, $3d$, $4s$, and $4p$ orbitals are optimized on the $2s2p3s$, $2s2p3p$, $2s2p3d$, $2s^24s$, and $2s^24p$ states. The $4d$ function is correlation type and is optimized on the $2s^2 2p\ ^2P^o$ ground state.

TABLE I. Excitation energies of the O^{3+} states included in the present 25-state R-matrix calculation.

State index	LS state	Energy (eV) Calculated	Energy (eV) Observed
1	$2s^2 2p\ ^2P^o$	0.0	0.0
2	$2s2p^2\ ^4P$	8.74	8.81[a]
3	$2s2p^2\ ^2D$	15.95	15.69[a]
4	$2s2p^2\ ^2S$	20.83	20.37
5	$2s2p^2\ ^2P$	22.79	22.39
6	$2p^3\ ^4S^o$	28.67	28.70
7	$2p^3\ ^2D^o$	31.84	31.64
8	$2p^3\ ^2P^o$	36.26	35.82
9	$2s^23s\ ^2S$	44.30	44.33
10	$2s^23p\ ^2P^o$	48.34	48.37
11	$2s^23d\ ^2D$	52.14	52.00
12	$2s2p3s\ ^4P^o$	54.40	54.42
13	$2s2p3s\ ^2P^o$	56.25	56.15
14	$2s2p3p\ ^2P$	57.94	57.92
15	$2s2p3p\ ^4D$	58.12	58.08
16	$2s2p3p\ ^4S$	58.87	58.81
17	$2s2p3p\ ^4P$	59.39	59.37
18	$2s2p3p\ ^2D$	59.96	59.98
19	$2s^24s\ ^2S$	60.14	60.22
20	$2s2p3p\ ^2S$	61.40	61.09
21	$2s2p3d\ ^4F^o$	61.44	61.40
22	$2s2p3d\ ^4D^o$	61.97	61.96
23	$2s2p3d\ ^2P^o$	62.02	61.98
24	$2s2p3d\ ^2D^o$	62.26	62.17
25	$2s2p3d\ ^4P^o$	62.49	62.49

[a]Take into account the fine-structure splitting of the ground state.

The convergence of CI expansions for different LS symmetries was tested by considering up to two electron excitations from the basic configurations $2s^2 2p$, $2s2p^2$, $2p^3$, $2s2p3s$, $2s2p3p$, $2s2p3d$, $2s^23s$, $2s^23p$, $2s^23d$, $2s^24s$, and $2s^24p$. The configurations with mixing coefficients less than 0.005 were then omitted from the CI expansions. In the final calculation the symmetries $^2P^o$, $^2D^o$, $^4S^o$, $^4P^o$, $^4P^o$, $^4F^o$, ^4D, ^4P, ^4S, ^2D, ^2P, and ^2S have been represented by 55, 30, 8, 20, 15, 13, 16, 11, 8, 43, 32, and 43 configurations, respectively which add up to a total of 279 configurations. The quality of target wave functions is assessed by comparing the calculated excitation energies with values available from the NIST compilation [16]. There is very good agreement between the calculated values and the NIST compilation, as shown in Table I.

The wave function describing the electron-ion system in the internal region surrounding the atom with $r \leqslant a$ is expanded in terms of energy-independent functions [17]

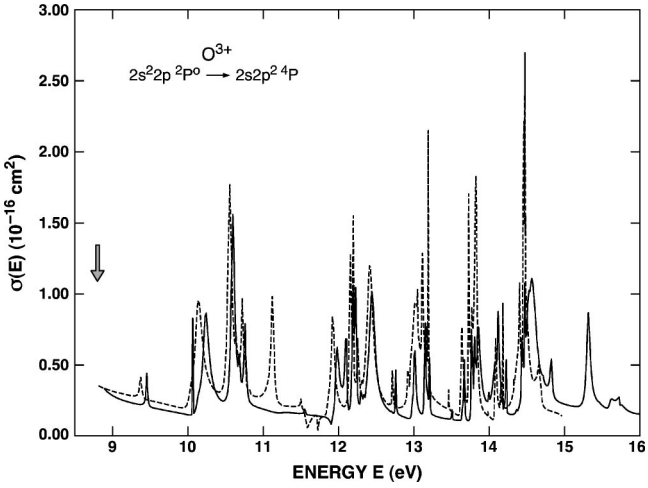

FIG. 2. Results of calculations for excitation of the $2s^2 2p\ ^2P^o \rightarrow 2s2p^2\ ^4P$ transition in O^{3+}. Shown are results in an eight-state R-matrix calculation [7] (dashed line) and present results in a 25-state R-matrix calculation (solid line). The arrow indicates the threshold for this transition at 8.810 eV.

$$\Psi_k = \mathsf{A} \sum_{ij} a_{ijk} \overline{\Phi}_i u_j(r) + \sum_j b_{jk} \phi_j , \tag{2}$$

where $\overline{\Phi}_i$ are channel functions formed from the multiconfigurational functions of the target states and u_j are the radial basis functions describing the motion of the scattering electron. The operator A antisymmetrizes the wave function, and a_{ijk} and b_{jk} are expansion coefficients determined by diagonalizing the $(N+1)$-electron Hamiltonian. The functions ϕ_j in Eq. (2) are of bound-state type and are included for completeness and to allow for short-range correlation effects. The radius of the R-matrix box was chosen to be $16.4a_0$ to accommodate all nine orbitals. A total of 28 continuum orbitals were used in each channel so that good convergence was obtained for electron energies of interest. The calculated target state energies were adjusted to the observed values prior to diagonalization in order to facilitate a more meaningful comparison of cross section with experiment. The R-matrix calculations were carried out for partial waves with $L=0-20$ using the R-matrix computer packages [17]. These partial waves were sufficient to obtain converged cross sections for the transitions considered here.

IV. RESULTS AND DISCUSSION

Shown in Fig. 2 are results of the present 25-state R-matrix calculation and the earlier 8-state R-matrix calculation of Luo and Pradhan [7] for the intersystem $2s^2 2p\ ^2P^o \rightarrow 2s2p^2\ ^4P$ transition in the energy region between the ^4P (8.810 eV) and ^2D (15.690 eV) thresholds. There is overall good agreement for the two transitions considered in the present work. There are several Rydberg series of resonances converging to the $2s2p^2\ ^2D$ threshold. The overlapping of these series makes the resonance structure complicated. The resonance structure in the calculation of Luo and Pradhan is shifted to the lower energy side. This shift may have been caused by the lower calculated value of the $2s2p^2\ ^4P$ threshold in their calculation (8.56 eV), as compared to present theory (8.74 eV) and to the spectroscopic value (8.810 eV). The background cross sections away from resonances in the present calculation are lower than those of the eight-state calculation. These discrepancies in the background cross sections are perhaps caused by the difference in target wave functions used in the two scattering calculations. There are also differences in the widths and peaks of resonances caused by the additional coupling to the higher excited states in the present work. It is clear that the resonances make substantial enhancements in the cross sections.

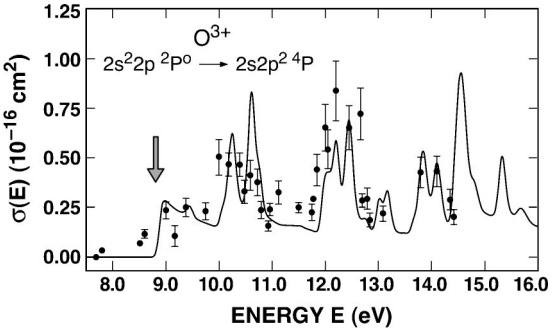

FIG. 3. Experimental and theoretically calculated cross sections for excitation of the $2s^2 2p\ ^2P^o \rightarrow 2s2p^2\ ^4P$ transition in O^{3+}. Error bars are total absolute errors at each energy. The solid circles and solid line are experimental and calculated results, respectively. The arrow indicates the threshold for this transition at 8.810 eV.

Results of the present 25-state R-matrix calculation and experimental measurements are shown in Figs. 3 and 4 for the $2s^2 2p\ ^2P^o \rightarrow 2s2p^2\ ^4P$ intersystem transition and the $2s^2 2p\ ^2P^o \rightarrow 2s2p^2\ ^2D$ resonance transition, respectively. The total error in the experimental data is 18% (1.7σ). The

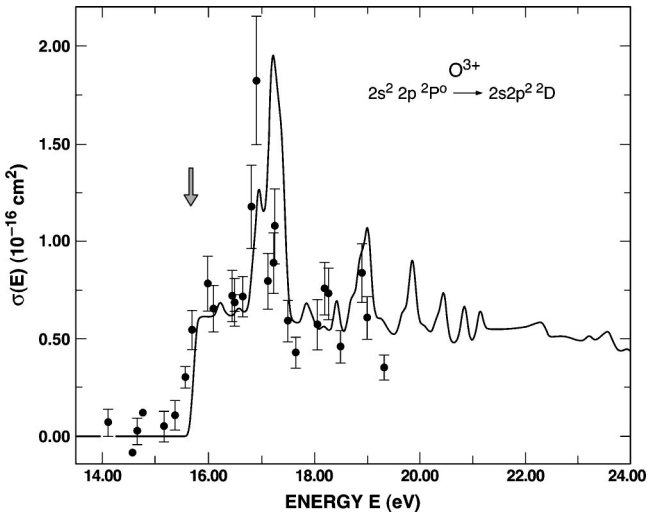

FIG. 4. Experimental and theoretically calculated cross sections for excitation of the $2s^2 2p\ ^2P^o \rightarrow 2s2p^2\ ^2D$ transition in O^{3+}. Error bars are total absolute errors at each energy. The solid circles and solid line are experimental and calculated results, respectively. The arrow indicates the threshold for this transition at 15.690 eV.

TABLE II. Absolute experimental excitation cross sections for the $2s^2 2p\ ^2P^o \rightarrow 2s2p^2\ ^4P$ and $2s^2 2p\ ^2P^o \rightarrow 2s2p^2\ ^2D$ transitions in O^{3+}. Threshold energies for the $^2P^o \rightarrow ^4P$ and $^2P^o \rightarrow ^2D$ transitions are 8.810 and 15.690 eV, respectively. Nonzero cross sections below threshold are due to the electron-energy spread in the primary beam. The unit of cross section is 10^{-16} cm^2.

$2s^2 2p\ ^2P^o \rightarrow 2s2p^2\ ^4P$ transition		$2s^2 2p\ ^2P^o \rightarrow 2s2p^2\ ^2D$ transition	
Energy E (eV)	$\sigma(E)$	Energy E (eV)	$\sigma(E)$
7.71	0.002	14.1	0.071
7.81	0.033	14.6	−0.082
8.51	0.071	14.7	0.032
8.60	0.119	14.8	0.119
9.00	0.237	15.2	0.051
9.17	0.108	15.4	0.107
9.38	0.252	15.6	0.302
9.75	0.232	15.7	0.543
9.99	0.503	16.0	0.781
10.2	0.467	16.1	0.653
10.4	0.465	16.4	0.718
10.5	0.329	16.5	0.686
10.6	0.413	16.6	0.714
10.7	0.377	16.8	1.18
10.8	0.238	16.9	1.82
10.9	0.158	17.1	0.794
10.9_6	0.240	17.2_3	0.888
11.1	0.326	17.2_5	1.08
11.5	0.251	17.5	0.592
11.7_5	0.227	17.6	0.431
11.7_7	0.294	18.1_6	0.572
11.8	0.439	18.2	0.757
12.0	0.652		
12.1	0.543		
12.2	0.837	18.3	0.731
12.4	0.652	18.5	0.459
12.6_6	0.721	18.9	0.837
12.7	0.285	19.0	0.607
12.7_9	0.295	19.3	0.354
12.8	0.187		
13.1	0.219		
13.8	0.426		
14.1	0.430		
14.3_5	0.289		
14.4	0.201		

component errors were: counting statistics; errors in F, L, I_e, I_i; metastable fraction in the ion beam, correction for the overlapping elastic contribution, and correction for overlapping between the two transitions at the energies above the opening of the $^2P^o \rightarrow ^2D$ transition at 15.690 eV [18]. The experimental values are listed in Table II. Each experimental value in Figs. 3, 4, and Table II is the result of 1–8 measurements.

In order to compare experiment and theoretical results at comparable resolutions, the theoretical results were further convoluted with an energy-dependent width ΔE taken from the experimental measurements. This resulted in a broadening of the calculated sharp and densely packed resonances structure, nevertheless leaving clearly defined resonance enhancements in the calculation. The width ΔE in the c.m. frame is simply given by $\Delta E = \Delta E_e[1 - 5.8343 \times 10^{-3}\ (E_i/E_e)^{1/2}]$ [18]. Here, ΔE_e is the electron energy width (full width at half maximum) in the laboratory frame, and E_e, E_i are the electron and ion laboratory energies, respectively. In the present case the O^{3+} ions were accelerated to an energy of $7.0q$ keV = 21.0 keV, and hence the broadening expression in terms of the electron laboratory energy is $\Delta E = \Delta E_e[1 - 0.84545/E_e^{1/2}]$. The value of ΔE_e is measured to be 0.104 eV.

Evidence for the strong resonance enhancement in cross section is clearly seen for each transition. For the lower-energy $^2P^o \rightarrow ^4P$ transition clear enhancements are seen at threshold, in the energy ranges 9.9–10.9, 11.8–12.7, and

near 14 eV. There is good agreement in energy location of the calculated and measured structures, consistent with the inherent width of the resonances and the error in the electron energy scale (0.1 eV). Measurements above 14.4 were affected by an elastically scattered electron contribution, and by overlap with the underlying $^2P^o \rightarrow {}^2D$ transition. The correction for the elastic scattering contribution to the inelastic signal, typically in the range 0–20 % (and accurate to about 5%), exceeded that for contribution from the underlying $P \rightarrow D$ transition. For example, taking the worst case of the $P \rightarrow P$ transition at 19.0 eV, correction for the elastic scattering contribution was 26%; whereas correction for the underlying $P \rightarrow D$ transition was only 3.7%. Results for the higher-energy and $^2P^o \rightarrow {}^2D$ transition (Fig. 3) again shows resonance enhancement due to multiple, sharp resonances in the range 16.7–17.5 eV. There appears to be a difference between experiment and theory, with the experimental maximum closer to 16.9 eV and calculations peaking near 17.2 eV. This difference could arise from (either or both) the fact that the resonance components contributing to the small shoulder at 17.0 eV are actually broader than calculated, hence are more easily resolved in the experiment; or that the main peak at 17.2 eV is calculated to be at an energy 0.2–0.3 eV too high. Although the calculated excitation thresholds have been adjusted to measured values, the calculated positions of resonances may still be slightly shifted compared to measured positions.

In summary, there is overall good agreement between absolute excitation cross section measurements for the O^{3+} $^2P^o \rightarrow {}^4P$ intersystem transition and the $^2P^o \rightarrow {}^2D$ resonance transition; and results of a 25-state R-matrix calculation. The agreement extended over energies from threshold to 1.6× and 1.2× threshold, respectively. This allows one to smoothly carry a theoretical calculation from higher energies (where merged-beams and energy-loss measurements are more difficult and calculations relatively easier) into the threshold region where the reverse is true. The large range of energies is important for modeling the large range of electron temperatures encountered in cool interstellar regions, hotter confined fusion plasma, solar corona, and the high-temperatures of solar flares and novae.

ACKNOWLEDGMENTS

J.A.L. thanks the National Academies of Science-National Research Council for support. S.S.T. was supported by NASA Grant No. NAG5-11434 from the Space Astrophysics Research and Analysis Program. The experimental work was carried out at the Jet Propulsion Laboratory, California Institute of Technology, and was supported under contract with the National Aeronautics and Space Administration.

[1] F. P. Keenan *et al.*, Mon. Not. R. Astron. Soc. **337**, 901 (2002).
[2] A. K. Bhatia, G. Doschek, and U. Feldman, Astron. Astrophys. **86**, 32 (1980).
[3] D. R. Flower and H. Nussbaumer, Astron. Astrophys. **45**, 145 (1975).
[4] G. M. Harper *et al.*, Mon. Not. R. Astron. Soc. **303**, L41 (1999).
[5] E. Sturm *et al.*, Astron. Astrophys. **393**, 821 (2002).
[6] M. Vestergaard and B. J. Wilkes, Astrophys. J., Suppl. Ser. **134**, 1 (2001).
[7] D. Luo and A. K. Pradhan, Phys. Rev. A **41**, 165 (1990).
[8] R. D. Blum and A. K. Pradhan, Astrophys. J., Suppl. Ser. **80**, 425 (1992).
[9] H. L. Zhang and A. J. Pradhan, Phys. Rev. A **50**, 3105 (1994).
[10] T. Brage, P. G. Judge, and P. Brekke, Astrophys. J. **464**, 1030 (1996).
[11] J. Zeng and J. Yuan, J. Phys. B **35**, 3041 (2002).
[12] J. B. Greenwood, S. J. Smith, A. Chutjian, and E. Pollack, Phys. Rev. A **59**, 1348 (1999).
[13] A. Chutjian, J. B. Greenwood, and S. J. Smith, in *Applications of Accelerators in Research and Industry*, edited by J. L. Duggan and I. L. Morgan (AIP, New York, 1999), p. 475.
[14] S. J. Smith, M. Zuo, A. Chutjian, S. S. Tayal, and I. D. Williams, Astrophys. J. **463**, 808 (1996).
[15] C. Froese Fischer, Comput. Phys. Commun. **64**, 369 (1991).
[16] See the NIST database at http://physics.nist.gov
[17] K. A. Berrington, W. B. Eissner, and P. H. Norrington, Comput. Phys. Commun. **92**, 290 (1995).
[18] S. J. Smith, J. B. Greenwood, A. Chutjian, and S. S. Tayal, Astrophys. J. **541**, 501 (2000).